Geophysical Journal (1988) **94**, 171–180

60.

Body-wave deconvolution for variable source parameters; application to the 1978 December 6 Kuriles earthquake

Paul R. Lundgren, Emile A. Okal and Seth Stein
Department of Geological Sciences, Northwestern University, Evanston, IL 60208, USA

Accepted 1987 November 23. Received 1987 November 23; in original form 1987 May 19

SUMMARY

A method to determine the depth and mechanism of subevents in earthquakes with complex rupture is developed. Complex body-waves are deconvolved using a damped Lanczos inversion to retrieve the source time function. Some constraints on the mechanism and depth of the first subevent are assumed, though not required. The data set is deconvolved using the Green's function for the first subevent to obtain a best-fitting source time function. This source time function is then windowed in time around the first pulse and the corresponding synthetic seismogram is subtracted from the data. This process is repeated on residual data to determine mechanisms and depths of subsequent subevents.

This method is applied to the 1978 December 6 Kuril Islands earthquake, a complex event which ruptured vertically from 100 to 220 km in depth, and represents tearing of the Pacific plate as it subducts beneath the Kuril and Honshu arcs. Using long-period WWSSN data, we found three main subevents with the mechanism $\phi = 150°$, $\delta = 80°$, and $\lambda = 20°$ at depths of 120, 165, and 210 km. In this particular case one nodal plane is very well constrained and there is some *a priori* evidence for significant vertical rupture.

Key words: Source-time function, deconvolution, vertical rupture

1 INTRODUCTION

Large earthquakes with ruptures of long duration involving large fault areas present a challenge in the determination of the details of the rupture. For large subduction zone events, rupture over a significant depth extent can occasionally result in substantial discrepancies between centroid depths determined from long-period surface waves and depths determined from first arrival times (Giardini 1984; Romanowicz & Guillemant 1984), the latter being presumably related to the depth of initial rupture. Inversion of long-period body-waves for the source time function is important for understanding the complexity of the rupture, the history of moment release and the spatiotemporal distribution of asperities or barriers (Kikuchi & Kanamori 1982; Ruff & Kanamori 1983; Nábělek 1984; Christensen & Ruff 1985).

A number of similar methods have been used for these purposes. One, due to Kikuchi & Kanamori (1982), builds up the source time function iteratively as a series of weighted pulses temporally located at the maximum of the cross-correlation between the residual seismogram and a synthetic wavelet for a ramp function. The sequence of pulses obtained after a given number of iterations is then convolved with the unit ramp to give the final source time function. This method has been used with considerable success in the retrieval of source parameters and source time history (Stein & Wiens 1986). However, these authors point out that its depth estimates become inaccurate for up-dip or down-dip rupture extending over a wide depth range. In addition, when inverting for complex source time functions lasting several tens of seconds, this method can lead to static offsets in the moment rate function, making it difficult to resolve the true source time function. A second method (Ruff & Kanamori 1983) is based on the least-squares inversion formalism of Lanczos (1961). In the Appendix, we discuss the relative performance of the two methods, and show that the least-squares method is theoretically more accurate, a feature becoming significant when trying to solve for pulses separated by short time intervals, or with substantial duration. We confirm this through an experiment on synthetics. An extension of the Kikuchi & Kanamori method solves for the source pulses both temporally and spatially on a fault of given geometry and dimensions (Kikuchi & Fukao 1985).

The above techniques usually assume a constant focal mechanism and depth. Similarly, in most moment tensor inversions of body waves (Stump & Johnson 1977; Dziewonski, Chou & Woodhouse 1981; Sipkin 1982), the time behaviour of all moment tensor components is usually taken as identical, resulting in a focal geometry invariant with time. Such assumptions may be inappropriate for large earthquakes with vertical rupture.

In a recent study, Kim & Wallace (1986) developed a

moment tensor inversion technique allowing differing time histories for the various components, which has been used to successfully model two complex Iranian earthquakes (Slevin & Wallace 1986). This method can occasionally lead to large non-double couple components.

In this paper, we develop a method for applying a damped Lanczos inversion to pure double couple earthquake sources of varying depth and geometry. Using this method for the 1978 December 6 Kuril Islands earthquake, we suggest an extended (≈90 km) vertical rupture.

2 OUTLINE OF THE LEAST SQUARES METHOD

A teleseismic body wave signal $s(t)$ can be represented as the convolution $s(t) = m(t)^* e(t)^* i(t)$, where $m(t)$ is the source time function, $e(t)$ is the impulse response of the Earth, a combination of its transfer function and of the source geometry, and $i(t)$ is the instrument response. Grouping $e(t)$ and $i(t)$ together, $s(t) = g(t)^* m(t)$, where $g(t)$ is the Green's function for a particular mechanism and depth. The convolution, in vector-matrix form is $s_i = G_{ij} m_j$ where $\mathbf{G}$ is the Green's function matrix.

We use a damped Lanczos inversion to solve for the source time function $\mathbf{m}$ in the least-squares sense (Lanczos 1961; Ruff & Kanamori 1983):

$$\mathbf{m} = \mathbf{G}^* \mathbf{s}, \tag{1}$$

with

$$\mathbf{G}^* = (\mathbf{G}^T \mathbf{W} \mathbf{G} + d\mathbf{I})^{-1} \mathbf{G}^T \mathbf{W}, \tag{2}$$

where $\mathbf{W} = \mathbf{I}[1/\mathrm{var}(\mathbf{s})]$ weights the inverted data set, d is the damping parameter and $\mathbf{I}$ is the identity matrix. This formalism is not restricted to a single station and can simultaneously invert a multiple station data set.

The application of the Lanczos inversion to complex body waves, which we will call the Least-squares method, is straightforward. At each step, the depth and fault geometry of an individual subevent in the source time function is chosen so as to miminize the squared error between residual data and synthetics. The synthetic seismogram for that subevent is then subtracted from the residual seismogram, and the process iterated for the next subevent. This procedure is stopped when the residual data set is reduced to the noise level in amplitude. The crucial difference between this approach and that of Kikuchi & Kanamori is that subevents are treated sequentially in time, rather than in relation to their moment release amplitude, thus providing stricter control on the time evolution of the focal geometry and depth.

3 APPLICATION OF METHOD TO SYNTHETIC DATA

In order to test this method, we generated synthetic *P*-wave data for a complex rupture consisting of two subevents with different mechanisms and depths. Fig. 1 shows the source time function and mechanisms used. The mechanism for the first pulse has a strike $\phi = 0°$, a dip $\delta = 45°$, and a slip $\lambda = 90°$, at a depth of 120 km. The second pulse has the same strike and dip but with $\lambda = 135°$ and a depth of 160 km.

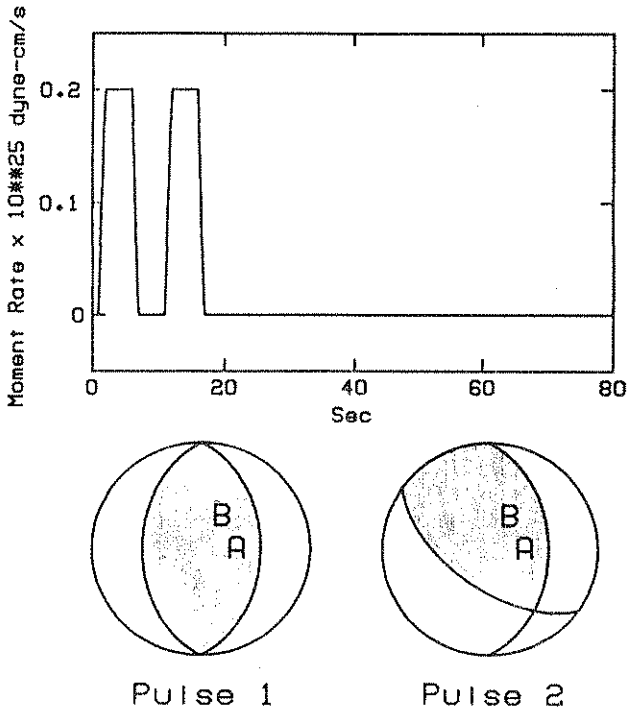

Figure 1. Source time function and mechanism of each pulse for synthetic data used as a test of the least-squares method. For pulse 1, $\phi = 0°$, $\delta = 45°$ and $\lambda = 90°$. For pulse 2, the strike and dip are the same but $\lambda = 135°$. Fault parameter convention is that of Kanamori & Cipar (1974). The locations of test stations A and B on focal mechanism plots are shown.

As a first step, we use the correct mechanism for the first pulse, and, assuming no change in mechanism during the rupture, deconvolve the data set for the whole source time function. (The mechanism of the first pulse controls the polarities of teleseismic first motions and, as such, can be expected to be known relatively accurately.) This procedure is carried out over a range of depths; for each depth, the synthetic seismogram $\mathbf{c} = \mathbf{G}\mathbf{m}$, with $\mathbf{m}$ given by (1), and squared residual $|\mathbf{s} - \mathbf{c}|^2$ are computed. The depth yielding the minimum residual is taken as the depth of the first pulse. Fig. 2(a) shows that this procedure retrieves it correctly at 120 km, although a strong local minimum exists around 200 km. The second minimum at 200 km while having nearly as low a residual value as that at 120 km has a significantly poorer source time function with a much larger amount of the curve having a negative moment rate. This would imply a succession of back-and-forth motions along the fault plane. Therefore the depth of 120 km is the minimum which gives a physically acceptable result for the first pulse. Fig. 3(a) shows the source time function computed for 120 km. Most noticeable is the development of a spurious third pulse (indicated by a question mark) 40 s into the source time function. If the inversion were stopped at this stage, an erroneous picture of the source process would emerge, since the total source duration would be taken as 45 s, rather than the correct 20 s. Inferences about the extent and structure of the fault zone, in particular regarding the existence of asperities, could be incorrect.

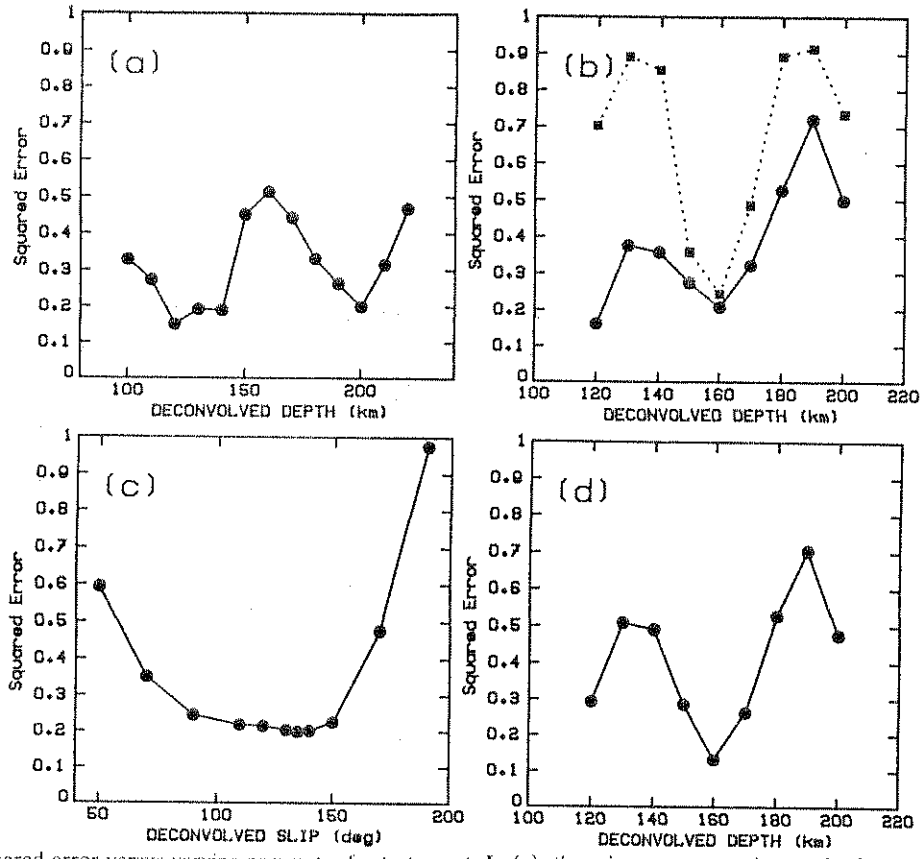

Figure 2. Plots of squared error versus varying parameter for test event. In (a), the seismograms are deconvolved over a range of depths using the mechanism for the first pulse. In (b), the residual is deconvolved using the mechanism for the first pulse for the whole source time function (solid line), and for a time-windowed source time function of 0–15 s (dashed line). In (c), the correct slip is found for the second pulse using the correct depth of 160 km obtained from (b). In (d), the residual is deconvolved over a range of depths using the correct mechanism for the second pulse. See text for details.

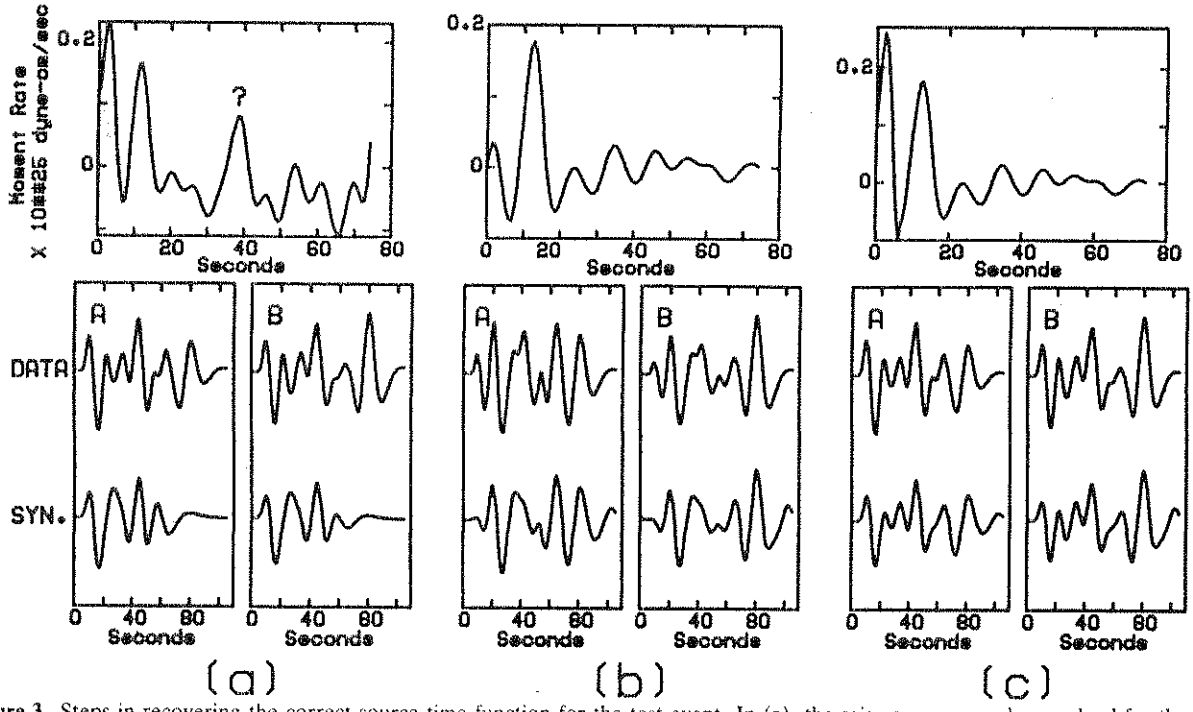

Figure 3. Steps in recovering the correct source time function for the test event. In (a), the seismograms are deconvolved for the mechanism and depth of the first pulse (shaded). Note the spurious third pulse (question mark). In (b), the residual data are deconvolved for the mechanism and depth of the second pulse. In (c), the first pulse in the source time function (a) and the whole source time function in (b) are summed to give the final source time function and the final synthetics. See text for details.

To allow for possible changes of focal parameters (geometry or depth) in the later pulses, we assume that the results of this first pass apply only to the first pulse [shaded on Fig. 3(a)]. We then compute a synthetic $\mathbf{c}^{(1)} = \mathbf{G}\mathbf{m}^{(1)}$, where $\mathbf{m}^{(1)}$ is the time function truncated after the first pulse (in this case 7 s) and obtain a residual signal $\mathbf{s}^{(1)} = \mathbf{s} - \mathbf{c}^{(1)}$, which can be interpreted as the contribution to the seismogram of all later pulses. In this notation, superscripts indicate the order of iteration; the superscript of order zero is dropped.

The second step is the estimation of the depth and mechanism for the second subevent. In principle, we seek the set of parameters in a 4-D space (ϕ, δ, λ; and depth h), which best fit the residual seismogram $\mathbf{s}^{(1)}$. In practice, we experimented with several strategies, and found that the source depth is the most robust parameter, which we therefore determine first. This is due to the fact that in the synthetic body wavetrain consisting of P, pP and sP, the depth controls the time intervals between the three arrivals, and thus affects the cross-correlation $\mathbf{G}^{\mathrm{T}}\mathbf{W}\mathbf{s}^{(1)}$ more significantly than does the geometry (ϕ, δ, λ), which controls the relative amplitude of the contributing rays (Stein & Wiens 1986). If a station were nodal for any of the later subevents the amplitudes of the direct (P) phase would be zero. This could cause a problem if only one station were used. Since we invert multiple stations simultaneously this potential problem can be averted.

The solid line in Fig. 2(b) shows the residual for the second iteration as a function of depth, using the geometry of the first subevent. This plot has two minima, one corresponding to the depth of the second pulse (160 km). The other one at the depth of the first pulse is a leftover artefact of the spurious pulse in the first iteration, which disappears if the synthetic $\mathbf{c}^{(2)}$ is computed by truncating the time function $\mathbf{m}^{(2)}$ resulting from the second inversion after 15 s. The corresponding residual versus depth for this case [the dashed line in Fig. 2(b)], exhibits a single minimum at the correct depth of the second pulse. By truncating the time function after 15 s, the residuals for depths greater and lesser than 160 km show a substantial increase since these depths require spurious pulses later in the source time function.

Similarly, Fig. 2(c) shows the fit of the 2nd iteration as a function of slip angle, for the correct depth of 160 km. This plot has a minimum at the correct slip angle, 135°, and also illustrates that the data set is much less sensitive to slip than to depth. Only grossly wrong mechanisms, resulting for example in a reversal of the polarity of the rays, are clearly unacceptable.

Figure 2(d), the analogue of Fig. 2(b) with the correct geometry for the second pulse, confirms the correct depth of the 2nd subevent (160 km).

Figure 3(b) shows the source time function resulting from deconvolving the residual data using the correct mechanism and depth of the second pulse.

After the second iteration the source time function shows no more subevents occurring later in time after the 2nd pulse and the residual seismograms do not have a significant amplitude. At this point the iterative search is stopped. Fig. 3(c) shows the final source time function. Comparison with Fig. 1 shows that in addition to the variation of focal geometry and depth, the time and amplitude history of the source are satisfactorily retrieved. The spurious pulse in Fig. 3(a) has disappeared.

4 APPLICATION TO THE 1978 DECEMBER 6, KURIL ISLANDS EARTHQUAKE

This large intermediate-depth earthquake ($m_b = 6.3$, $M_S = 7.1$) is particularly interesting since it is located at the junction of the Kuril and Honshu arcs (Fig. 4), where a change in the dip angle of the subduction causes a contortion or tearing of the plate (Isacks & Molnar 1971; Sasatani 1976). Comparable events may have occurred at the same location in 1907, 1924, 1945, and 1957. Several authors have studied this event with substantially varying results, in particular regarding its depth (Malgrange & Okal 1983; Silver & Jordan 1983; Romanowicz & Guillemant 1984; Giardini 1984; Kasahara & Sasatani 1985). The centroids found by inversion of ultra-long-period surface waves [176 km (Giardini 1984); 170 km (Romanowicz & Guillemant 1984)], are significantly deeper than the first motion hypocenters reported by the ISC (118 km) and NEIS (91 km). These discrepancies suggest a large vertical extent for the rupture. The aftershock distribution for this event also supports this concept since it extends vertically from 100 to 220 km (Fig. 5). A complex earthquake with three separate subevents extending over 70 s was found by Malgrange & Okal (1983) assuming constant depth and mechanism using the Kikuchi & Kanamori (1982) method.

Focal mechanism

Figure 6 shows the P-wave first motion mechanism which we determined for this event. All first motions plotted on this figure were read as part of this study. The NNW–SSE-trending plane is very well constrained. The aftershock

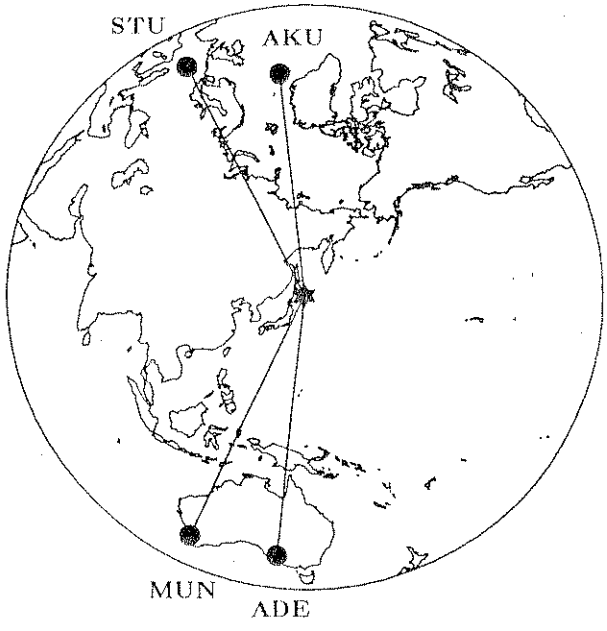

Figure 4. Location of the 1978 December 6, Kurile event (star) and the WWSSN stations used in this study (dots).

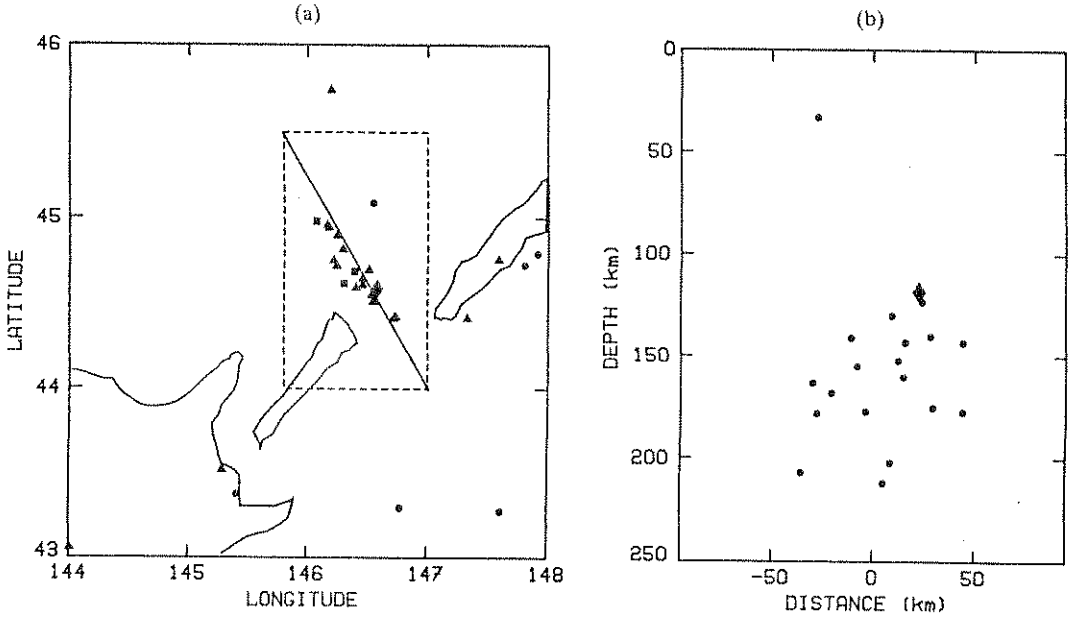

Figure 5. Locations of the main shock (square) and of the aftershocks (dots) of the 1978 sequence. (a) Map view showing the NW–SE trends of the aftershocks which indicate the trend of the fault plane. (b) Vertical cross-section along line parallel to the aftershock trend.

distribution suggests that this is the fault plane, which can be interpreted as the shear surface between the two slabs (see Fig. 5). On the other hand, the slip angle on this plane cannot be constrained by first motions alone. The mechanism shown on Fig. 6 results from our body-wave deconvolution.

Body-wave deconvolution

To apply the least-squares method to *P*-waves from this earthquake, we selected the four stations shown on Fig. 4, for which high-quality WWSSN data were available. All four stations were simultaneously deconvolved using 140 s of data to obtain 100 s of source time function.

The residual curves for each step are shown in Fig. 7 with the final results shown in Fig. 8. The range of trial source depths was taken from 100 to 220 km as suggested by the aftershock distribution. The depth of the first subevent was found at 120 km, in agreement with the ISC depth. The data were then deconvolved at 120 km to determine the best slip angle on the constrained fault plane ($\phi = 150°$, $\delta = 80°$). The slip angle minimizing the residual is $\lambda = 20°$, and the resulting mechanism is shown in Fig. 6.

The process was iterated further as described in Section 3. The final source time function has three or four major subevents with an increase in depth between each subevent. The first one at 120 km, is well defined and has a duration of approximately 15 s. The second one is much larger; it occurs at 165 km and is over 20 s in duration. The final part of the source time function, beyond 43 s, gave an error minimum at a depth of 210 km. The complex structure of the second subevent suggests that it may itself be split into several sources. When testing this possibility, we could not resolve a depth difference between its two parts, and thus treat it as a single subevent.

No change in focal mechanism between subevents was found to be resolvable by this data set. The resulting mechanism ($\lambda = 20°$) compares favourably with those of Giardini (1984) ($\phi = 322°$, $\delta = 85°$, $\lambda = -34°$), Romanowicz & Guillemant (1984) ($\phi = 338°$, $\delta = 86°$, $\lambda = -15°$), and Kasahara & Sasatani (1985) ($\phi = 150°$, $\delta = 80°$, $\lambda = 40°$).

We obtained seismic moments of 1.1, 2.0, and 2.3×10^{27} dyne-cm for each subevent, for a total of $(5.4 \pm 0.5) \times 10^{27}$ dyne-cm. This is substantially higher than the value of 2.5×10^{27} dyne-cm determined by Kasahara & Sasatani (1985) but well within the range of the CMT values (4×10^{27}, 3.6×10^{27}, and 6.3×10^{27} dyne-cm) determined by Giardini (1984), Silver & Jordan (1983), and Romanowicz & Guillemant (1984), respectively. The centroid of our three pulses is found at 175 km, in agreement with centroids determined from surface waves. Our value is only approximate since our choice of damping parameter ($d = 0.01$) can affect the final moment. Lesser damping increases the moment by allowing the source time function to be more 'jagged' and improves the fit between synthetics and data. Greater damping lowers the moment by smoothing the source time function and increases the squared error between the synthetic seismograms and the data.

Tectonic implications

The variation in depth during the source process of the 1978 Kuril event suggests that the nodal plane ($\phi = 150°$, $\delta = 80°$) was the fault plane. The direction of rupture inferred from the slip angle ($\lambda = 20°$) is generally consistent with the tearing motion of the plate at the subduction corner [Fig. 6(b)]. Fig. 6(c) shows that the dips of 40° beneath the Sendai arc and 50° beneath the Kuril arc call for a slip angle of 45°.

Finally, for this particular geometry involving shear between two subduction arcs, our study suggests the existence of a fault plane along which stress release takes place in a series of jagged pulses, which may correspond to regions of stronger coupling (possibly 'asperities'), in a

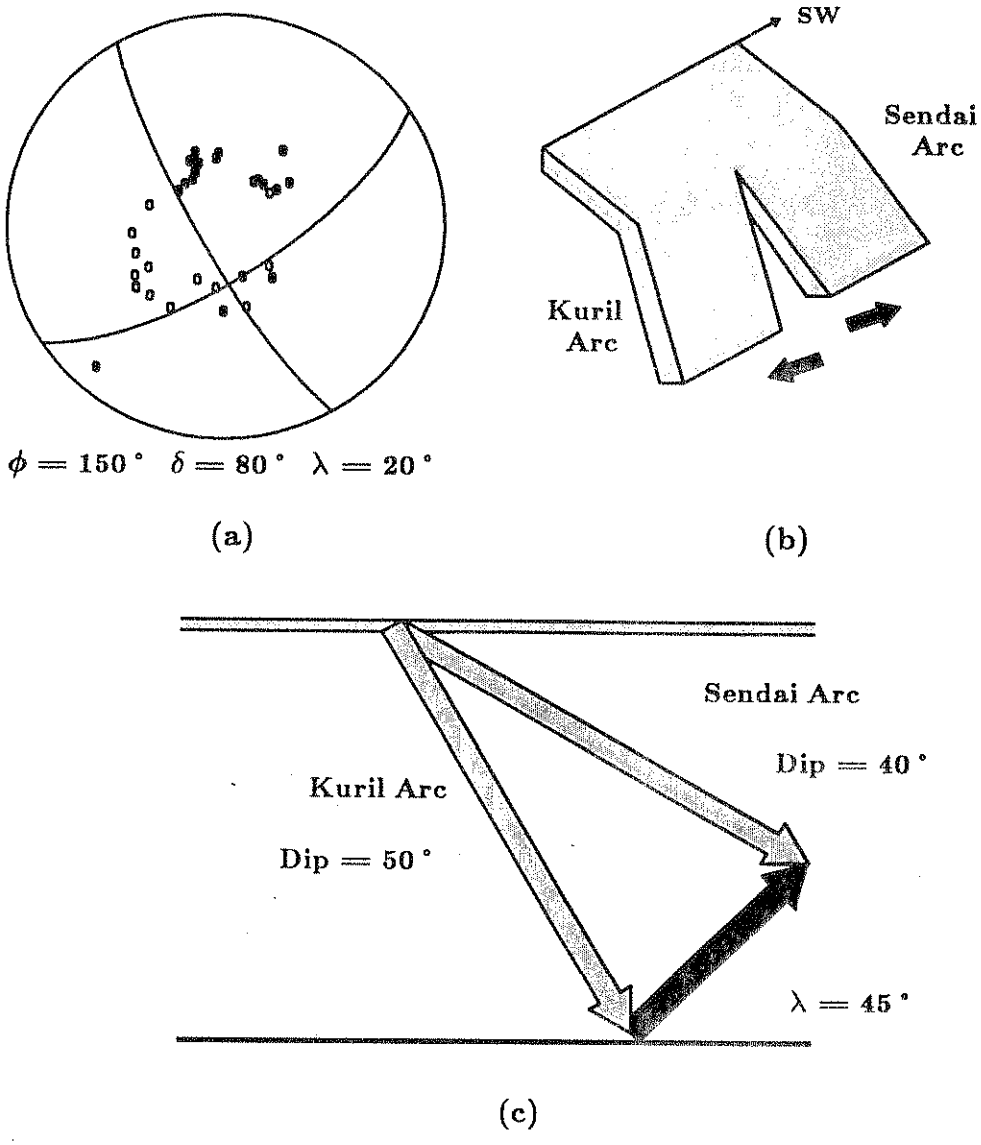

Figure 6. (a) P-wave first motion focal mechanism plot. Filled circles indicate compressional and open circles indicate dilatational first motions. (b) Sketch of tectonic interpretation of event. (c) Vector diagram showing expected slip angle ($\lambda = 45°$) between the Sendai slab (dip = 40°) and the Kuril slab (dip = 50°).

fashion not significantly different from that documented for shallow events. The vertical propagation velocities between subevents (2–3 km s^{-1}) are within the range of documented values for shallower ruptures.

5 CONCLUSIONS

We have presented a method for determining the depth and mechanism changes between subevents in complex events. The determination of the depth and mechanism of successive subevents is done by simultaneously inverting multiple station seismograms for the source time function and then, at each iteration, subtracting the synthetic seismograms for that subevent at the depth which gives a minimum error. Tests with synthetic data show that this method retrieves the depth correctly for a secondary subevent even with large errors in the focal mechanism for that subevent.

We applied this method to the 1978 December 6, Kuril Islands event, and obtained results which agree well with ISC and moment tensor inversion depths. The depths of the subevents suggest that the shallow ISC hypocentre represents the first pulse in the source time function. The much greater depths obtained from ultra-long-period surface waves and long-period body waves are explained by the deeper pulses. A comparison of our final source time function with that of Malgrange & Okal (1983) shows that our source time function has significant amplitude to approximately 90 s while that of Malgrange & Okal extends to over 120 s for some stations and the times of their second and third pulses are progressively later in time. This would be expected with a fixed depth of 120 km for the whole source time function.

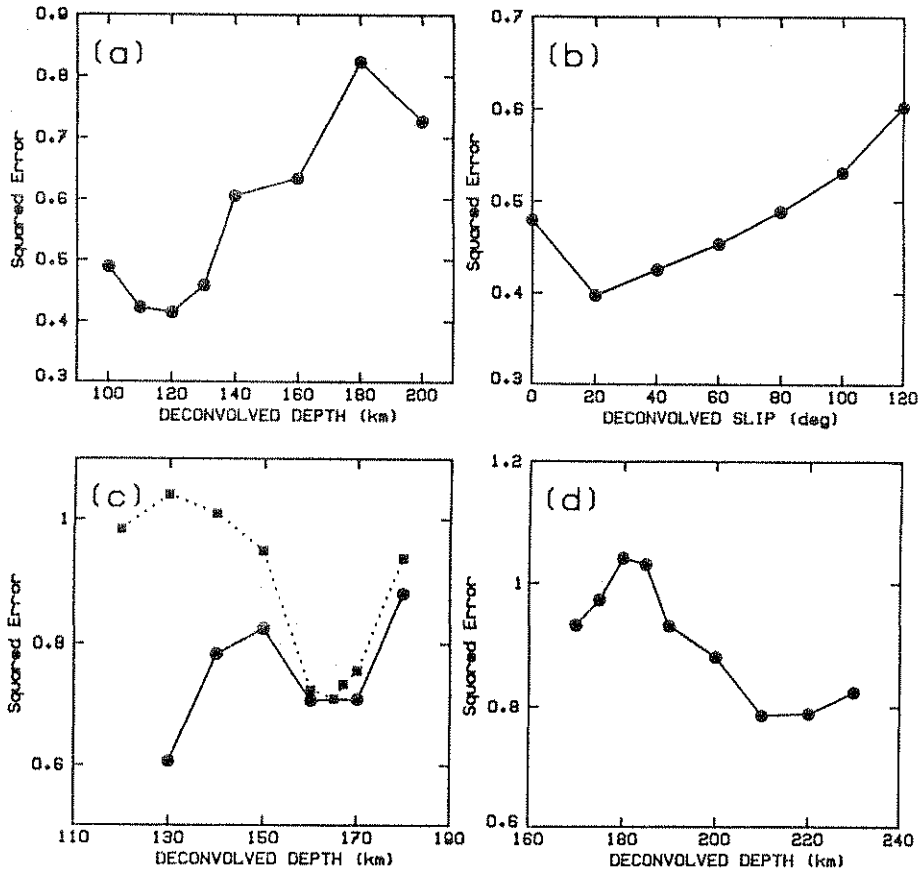

Figure 7. Plots of squared error versus varying parameter for Kuril event. In (a), the seismograms are deconvolved and the error is plotted for the whole source time function. In (b), the slip is found for the first pulse. In (c), the residual data are deconvolved to determine the depth of the second pulse. The solid line is for the whole source time function and the dashed line is for the part of the source time function corresponding only to the second pulse. In (d), the depth of the third pulse is found using a time window extending over the remaining part of the source time function.

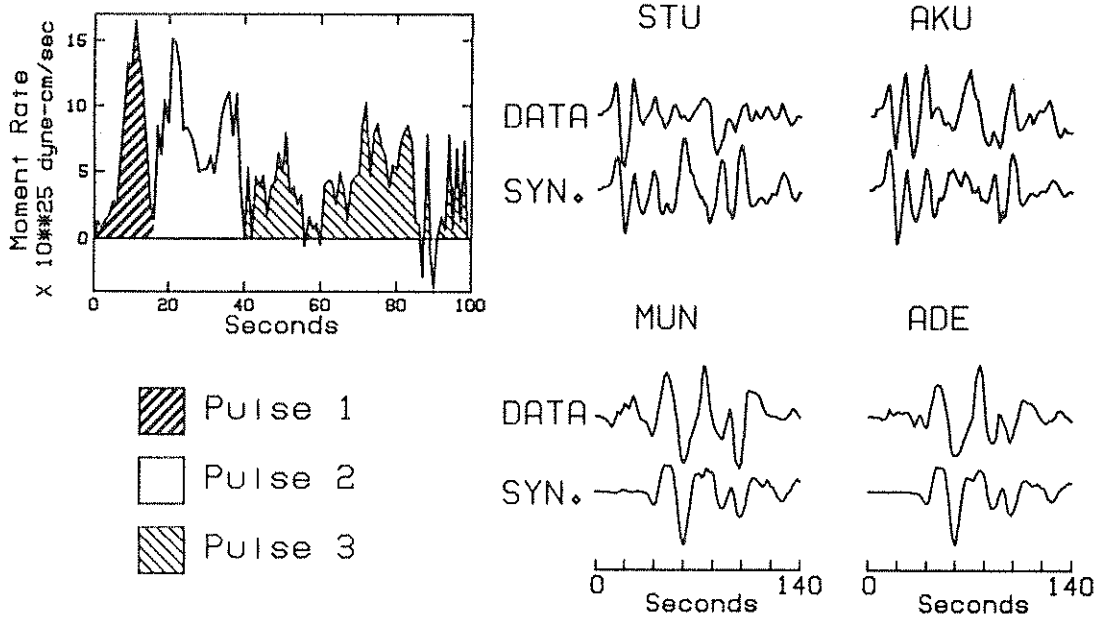

Figure 8. Final results for the Kuril event. On the left is the final source time function. The first pulse with a depth of 120 km extends from 0 to 16 s. The second pulse with a depth of 165 km extends from 16 to 40 s. The remainder of the source time function corresponds to a depth of 210 km. On the left are the data and final synthetics for the four stations used in the inversion.

ACKNOWLEDGMENTS

We are grateful to Larry Ruff for pointing out an inconsistency in a previous version of the paper. We also thank Doug Wiens for help in the initial stages of this research. This work was supported by the National Science Foundation, under grants EAR-84-05040 to E. A. Okal, and EAR-86-18038 to Seth Stein.

REFERENCES

Christensen, D. H. & Ruff, L. J., 1985. Analysis of the trade-off between hypocentral depth and source time function, *Bull. seism. Soc. Am.*, **75,** 1637–1656.

Dziewonski, A. M., Chou, T.-A. & Woodhouse, J. H., 1981. Determination of earthquake source parameters from waveform data for studies of global and regional seismicity, *J. geophys. Res.*, **86,** 2825–2852.

Giardini, D., 1984. Systematic analysis of deep seismicity: 200 centroid-moment tensor solutions for earthquakes between 1977 and 1980, *Geophys. J. R. astr. Soc.*, **77,** 883–914.

Isacks, B. & Molnar, P., 1971. Distribution of stresses in the descending lithosphere from a global survey of focal-mechanism solutions of mantle earthquakes, *Rev. Geophys. Space Phys.*, **9,** 103–174.

Kanamori, H. & Cipar, J. J., 1974. Focal process of the great Chilean earthquake May 22, 1960, *Phys. Earth planet. Int.*, **9,** 128–136.

Kasahara, M. & Sasatani, T., 1985. Source characteristics of the Kunashiri strait earthquake of December 6, 1978 as deduced from strain seismograms, *Phys. Earth planet. Int.*, **37,** 124–134.

Kikuchi, M. & Fukao, 1985. Iterative deconvolution of complex body waves from great earthquakes – the Tokachi – Oki earthquake of 1968, *Phys. Earth planet. Int.*, **37,** 235–248.

Kikuchi, M. & Kanamori, H., 1982. Inversion of complex body waves, *Bull. seism. Soc. Am.*, **72,** 491–506.

Kim, J. & Wallace, T. C., 1986. A comparison of moment tensor inversion techniques: time dependent and time independent moment tensor elements (abstract), *Eos, Trans. Am. geophys. Un.*, **67,** 1104.

Lanczos, C., 1961. *Linear Differential Operators,* Van Nostrand, London.

Malgrange, M. & Okal, E. A., 1983. Seismological investigations of a slab-tearing event (Abstract), *Eos, Trans. Am. geophys. Un.*, **64,** 262.

Nábělek, J. L., 1984. Determination of earthquake source parameters from inversion of body waves, *PhD thesis,* Massachusetts Institute of Technology, Cambridge.

Romanowicz, B. & Guillemant, P., 1984. An experiment in the retrieval of depth and source mechanism of large earthquakes using very long period Rayleigh-wave data, *Bull. seism. Soc. Am.*, **74,** 417–437.

Ruff, L. & Kanamori, H., 1983. The rupture process and asperity distribution of three great earthquakes from long-period diffracted P waves, *Phys. Earth planet. Int.*, **31,** 202–230.

Sasatani, T., 1976. Mechanism of mantle earthquakes near the junction of the Kurile and northern Honshu arcs, *J. Phys. Earth*, **24,** 341–354.

Silver, P. G. & Jordan, T. H., 1983. Total-moment spectra of fourteen large earthquakes, *J. geophys. Res.*, **88,** 3273–3293.

Sipkin, S. A., 1982. Estimation of earthquake source parameters by the inversion of waveform data: Synthetic waveforms, *Phys. Earth planet. Int.*, **30,** 242–259.

Slevin, J. H. & Wallace, T. C., 1986. Time dependent moment tensor inversion of the June 11, 1981 Golbaf and July 28, 1981 Sirch earthquakes in southern Iran, *Eos, Trans. Am. geophys. Un.*, **67,** 1104.

Stein, S. & Wiens, D., 1986. Depth determination for shallow teleseismic earthquakes: Methods and results, *Rev. Geophys. Space Phys.*, **24,** 806–832.

Stump, B. W. & Johnson, L. R., 1977. The determination of source properties by the linear inversion of seismograms, *Bull. seism. Soc. Am.*, **67,** 1489–1502.

APPENDIX: COMPARISON BETWEEN LEAST-SQUARES AND KIKUCHI & KANAMORI (1982) METHODS

In this appendix, we evaluate critically the relative performance of the body-wave inversion method of Kikuchi & Kanamori (1982) and of the least-squares method.

Both methods attempt to solve for $\mathbf{m}$ in $\mathbf{s} = \mathbf{Gm}$, where $\mathbf{m}$ is the sequence of weighted pulses giving the source function when convolved with a unit ramp, $\mathbf{G}$ is the Green's function matrix, and $\mathbf{s}$ the seismogram. In this appendix the Green's function, $\mathbf{G}$, for the least-squares method has been convolved with a unit ramp to make it the same as the Green's function of Kikuchi & Kanamori.

The undamped Lanczos inversion uses the well-known least-squares equation

$$\mathbf{m}_{Inv} = (\mathbf{G}^{\mathbf{T}}\mathbf{G})^{-1}\mathbf{G}^{\mathbf{T}}\mathbf{s}. \tag{A.1}$$

The Kikuchi & Kanamori deconvolution, rather than solve for the source time function in a single computation, builds it iteratively. The cross-covariance, $\mathbf{G}^{\mathbf{T}}\mathbf{s}$, between the seismogram and a synthetic for a ramp function is formed, and its largest component retained; let $t^{(1)}$ be the time at the corresponding point in the time series. The first pulse is then given by $\mathbf{m}^{(1)} = m^{(1)}\mathbf{e}^{(1)}$, where $\mathbf{e}^{(1)}$ is the unit vector consisting of a single pulse of unit amplitude at time $t^{(1)}$, and the amplitude $m^{(1)}$ of the pulse is given by

$$m^{(1)} = \frac{\mathbf{e}^{(1)\mathbf{T}} \cdot \mathbf{G}^{\mathbf{T}}\mathbf{s}}{\mathbf{e}^{(1)\mathbf{T}}\mathbf{G}^{\mathbf{T}} \cdot \mathbf{G}\,\mathbf{e}^{(1)}}, \tag{A.2}$$

the matrix form of Kikuchi & Kanamori's (1982) equation (12). The residual seismogram is then formed by subtraction:

$$\mathbf{s}^{(1)} = \mathbf{s} - \mathbf{G}\,\mathbf{m}^{(1)} \tag{A.3}$$

and the process iterated. Because (A.2) has the properties of a projector, it is easy to verify that $\mathbf{G}^{\mathbf{T}}\mathbf{s}^{(1)}$ is orthogonal to $\mathbf{e}^{(1)}$, and thus $\mathbf{m}^{(2)} = m^{(2)}\mathbf{e}^{(2)}$ is built at a time $t^{(2)} \neq t^{(1)}$. The final Kikuchi & Kanamori solution is

$$\mathbf{m}_{KK}^{(I)} = \sum_{i=1}^{I} m^{(i)}\mathbf{e}^{(i)} \tag{A.4}$$

where I is the total number of iterations performed.

In order to illustrate the relative performance of the two methods, we study theoretically the inversion of 'synthetic data', i.e. we assume that the signal $\mathbf{s}$ consists of a synthetic due to two pulses of amplitudes α_1 and α_2 (with $\alpha_1 > \alpha_2$), at times t_1 and t_2:

$$\mathbf{s} = \mathbf{G}[\alpha_1\mathbf{e}^{(1)} + \alpha_2\mathbf{e}^{(2)}]. \tag{A.5}$$

In the absence of any noise in the signal, the least-squares method retrieves the exact source:

$$\mathbf{m}_{Inv} = (\mathbf{G}^{\mathbf{T}}\mathbf{G})^{-1}\mathbf{G}^{\mathbf{T}}\mathbf{s} = \alpha_1\mathbf{e}^{(1)} + \alpha_2\mathbf{e}^{(2)}. \tag{A.6}$$

On the other hand, the Kikuchi & Kanamori method computes

$$\mathbf{G}^{\mathbf{T}}\mathbf{s} = \alpha_1\mathbf{G}^{\mathbf{T}}\mathbf{G}\mathbf{e}^{(1)} + \alpha_2\mathbf{G}^{\mathbf{T}}\mathbf{G}\mathbf{e}^{(2)}. \tag{A.7}$$

The largest component of this vector can depend on the characteristics of the matrix $\mathbf{G}^{\mathbf{T}}\mathbf{G}$, and may not always be along $\mathbf{e}^{(1)}$. However, even if the time t_1 of the first pulse is

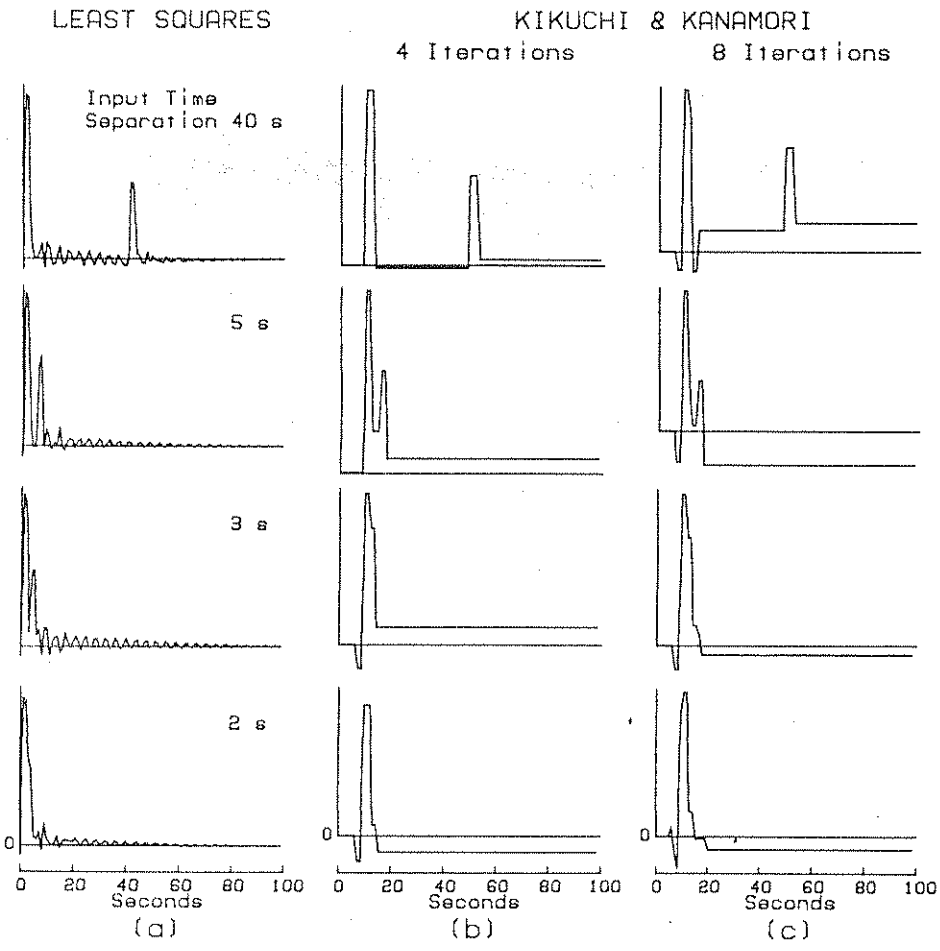

Figure A.1. Comparison of the performance of the least-squares and Kikuchi & Kanamori methods studied in the case of synthetic data. In all cases, we invert synthetic seismograms obtained from a source consisting of two pulses separated by a time by δt varying from 40 s (top) to 2 s (bottom). (a): Result of least-squares method. Note that the second pulse is retrieved with correct amplitude and time shift in all cases. (b): Result of four Kikuchi & Kanamori iterations. Note poor resolution for $\delta t = 2$ and 3 s. (c): Result of eight iterations. Note generally poor resolution of second pulse, and of relative amplitudes.

correctly obtained, this algorithm fails to directly retrieve its correct amplitude, but rather yields:

$$m_1 = \frac{\mathbf{e}^{(1)\mathrm{T}}\mathbf{G}^{\mathrm{T}}\mathbf{s}}{\mathbf{e}^{(1)\mathrm{T}}\mathbf{G}^{\mathrm{T}}\mathbf{G}\mathbf{e}^{(1)}} = \alpha_1 + \alpha_2 \cdot \frac{\mathbf{e}^{(1)\mathrm{T}}\mathbf{G}^{\mathrm{T}}\mathbf{G}\mathbf{e}^{(2)}}{\mathbf{e}^{(1)\mathrm{T}}\mathbf{G}^{\mathrm{T}}\mathbf{G}\mathbf{e}^{(1)}}, \tag{A.8}$$

and if the second pulse is retrieved through iteration 2 at the correct time t_2, its amplitude is given as

$$m_2 = \alpha_2 \left\{ 1 - \frac{[\mathbf{e}^{(2)\mathrm{T}}\mathbf{G}^{\mathrm{T}}\mathbf{G}\mathbf{e}^{(1)}]^2}{[\mathbf{e}^{(2)\mathrm{T}}\mathbf{G}^{\mathrm{T}}\mathbf{G}\mathbf{e}^{(2)}][\mathbf{e}^{(1)\mathrm{T}}\mathbf{G}^{\mathrm{T}}\mathbf{G}\mathbf{e}^{(1)}]} \right\}. \tag{A.9}$$

In addition, the times at which the vector $\mathbf{G}^{\mathrm{T}}\mathbf{s}$ is maximum may, under certain conditions, be improperly restored. The situation becomes increasingly complex if the real source is composed of a large number of pulses.

While it can be shown that the subsequent iterations of the method can correct the values of m_1 and m_2, the convergence of this correction is controlled by the off-diagonal terms of the matrix $\mathbf{G}^{\mathrm{T}}\mathbf{G}$. In practice, this means that the Kikuchi & Kanamori method should work well and fast if the source contains several well-separated pulses, but is not adequate if the separation between pulses is short or if the pulses are of long duration.

This theoretical result is upheld in the experiment shown in Fig. A.1: we invert 'synthetic data' obtained at two stations from a 45°-thrust fault source consisting of two pulses separated by a variable time interval δt. The amplitude of the second pulse is half that of the first one. The duration of the pulses is 3 s, the instrument involved is a WWSSN 15-100, so that the characteristic duration of the Green's function response is ~20 s. The various lines in figures correspond to different δt, from 40 s at top to 2 s at the bottom. In all cases, the least-squares method (*a*) extracts both pulses with an acceptable time and amplitude relationship; even in the case of the shortest time separation, a bulge is clearly present in the resulting inverted source function. On the other hand, the Kikuchi & Kanamori method fails to resolve the second pulse for the short separations ($\delta t = 2$ and 3 s), and retrieves the amplitudes incorrectly except for the longest separation. An increased number of iterations does not significantly improve its performance.

In principle, the Kikuchi & Kanamori method can be amended in the following way, to ensure convergence on the least-squares solution after a number of iterations N equal to the dimension of the parameter space: at the second

iteration, seek a vector $\mathbf{m}^{(2)}$ having components both along the previous unit vector $\mathbf{e}^{(1)}$, and along the largest component of $\mathbf{G}^T\mathbf{s}^{(1)}$ [say, $\mathbf{e}^{(2)}$], such that

$$\mathbf{G}^T\mathbf{s}^{(2)} = \mathbf{G}^T[\mathbf{s}^{(1)} - \mathbf{G}\mathbf{m}^{(2)}] \tag{A.10}$$

is orthogonal to both $\mathbf{e}^{(1)}$ and $\mathbf{e}^{(2)}$ [in the standard Kikuchi & Kanamori method, $\mathbf{G}^T\mathbf{s}^{(2)}$ is orthogonal only to $\mathbf{e}^{(2)}$]; this requires solving a 2×2 system. At the third iteration, seek $\mathbf{m}^{(3)}$ such that $\mathbf{G}^T\mathbf{s}^{(3)}$ is orthogonal to $\mathbf{e}^{(1)}$, $\mathbf{e}^{(2)}$, $\mathbf{e}^{(3)}$, etc. Under these conditions, the final residual, $\mathbf{s}^{(I)}$ is such that $\mathbf{G}^T\mathbf{s}^{(I)}$ is orthogonal to all vectors $\mathbf{e}^{(i)}$ $\{i = 1, 2, \ldots, I\}$.

If one were to apply the least-squares method to the residual vector $\mathbf{s}^{(1)}$ defined in (A.3), it is easily shown that the resulting source time function $\mathbf{m}^{(1)}_{\text{Res}}$ would be:

$$\begin{aligned}\mathbf{m}^{(1)}_{\text{Res}} &= (\mathbf{G}^T\mathbf{G})^{-1}\mathbf{G}^T\mathbf{s} - (\mathbf{G}^T\mathbf{G})^{-1}\mathbf{G}^T\mathbf{G}\mathbf{m}^{(1)} \\ &= \mathbf{m}_{\text{Inv}} - m^{(1)}\mathbf{e}^{(1)},\end{aligned} \tag{A.11}$$

this result being easily extended by induction. In particular, if we carry the amended Kikuchi & Kanamori method as described above to N iterations, where N is the length of the time series of the source,

$$\mathbf{m}^{(N)}_{\text{Res}} = \mathbf{m}_{\text{Inv}} - \sum_{i=1}^{N} m^{(i)}\mathbf{e}^{(i)}. \tag{A.12}$$

However, following the above remark, $\mathbf{G}^T\mathbf{s}^{(N)}$, which must be orthogonal to all N unit vectors in the space, is identically zero; therefore $\mathbf{m}^{(N)}_{\text{Res}}$ also is, and (A.6) becomes

$$\mathbf{m}_{\text{Inv}} = \sum_{i=1}^{N} m^{(i)}\mathbf{e}^{(i)}, \tag{A.13}$$

which proves the identity of the two methods if the least-squares method is neither damped nor weighted and the amended Kikuchi & Kanamori inversion is carried to a number of iterations identical with the dimension of the source space. In practice, this is never done, due to the very large amount of computation required for the full, amended, Kikuchi & Kanamori method; in particular in this method, the order of the linear system to be solved at each iteration increases with the number of the iteration; if the method is carried to $I = N$, the final system is $N \times N$; at this stage, the method bears no computational advantage over the exact inversion (A.1).

In conclusion, there exist systematic differences between the two methods, which can become very significant when inverting for pulses with short separation or long duration, as demonstrated by the experiment in Fig. A.1. In such cases, amending the Kikuchi & Kanamori method to ensure convergence is usually not a feasible alternative, due to the amount of computation, which fast becomes prohibitive. Additional differences may evolve from the weighting and damping chosen for the least-squares method. In practice the weighting matrix is determined at each step by the variance of the data. As is common in inverse procedures, the choice of the damping parameter is directly linked to the compromise between the desired stability and resolution, in the present case between the identification of individual sources and the regularity of the moment rate function.